The effect of mantle composition on density in the extending lithosphere

Nina S.C. Simon *, Yuri Yu. Podladchikov

Physics of Geological Processes, University of Oslo, P.O.Box 1048 Blindern, N-0316 Oslo, Norway

ARTICLE INFO

ABSTRACT

The density distribution of the lithosphere is non-linear and discontinuous due to complex mineralogy and, most importantly, phase transitions. We evaluate the influence of changes in mantle composition on lithospheric density and its evolution during horizontal stretching, using thermodynamic calculations of the density as a function of pressure, temperature and composition. We also develop a simple parameterization based on end-member mineral reactions and geometric relationships between the geotherm and the phase boundary for comparison. The garnet–spinel peridotite transition leads to a moderate decrease in density of the mantle part of the lithospheric column at the initial stages of stretching. When the crust is sufficiently thinned and temperature is relatively high, plagioclase peridotite becomes stable in the upper part of the mantle. The density reduction due to the plagioclase-in reaction is controlled by bulk Al_2O_3 in the mantle and by the depth of the plagioclase-in reaction, which is mainly governed by the Na_2O/Al_2O_3 ratio. Since Na_2O and Al_2O_3 increase with the fertility of the mantle the phase transition effect is most pronounced for relatively fertile mantle (and strong extension) and can lead to 2.3% density reduction. This is equivalent to heating the entire lithosphere by 700 °C if only the effect of thermal expansion on density is taken into account. The formation of plagioclase peridotite can explain syn-rift uplift in sedimentary basins that experienced large mantle stretching without invoking an unrealistically strong increase in temperature. It might also be responsible for the break-up unconformity observed at continental margins.

© 2008 Elsevier B.V. All rights reserved.

1. Introduction

Studies of mantle xenoliths and exposed mantle sections (ophiolites, peridotite massifs) have clearly shown that the Earth's lithospheric mantle spans a wide range of compositions (see reviews by Bodinier and Godard, 2003; Pearson et al., 2003). These compositional variations affect the density of the lithosphere in two ways: i) melt extraction from a more fertile precursor reduces the bulk density through removal of heavy elements like iron, while melt/fluid addition (metasomatism) has the opposite effect (Boyd and McCallister, 1976; Poudjom Djomani et al., 2001; Schutt and Lesher, 2006); ii) changing whole rock compositions lead to different mineral compositions and modal mineralogy due to complex petrological reactions (Green and Ringwood, 1970a,b; Ringwood, 1975). For example, higher aluminium contents lead to a greater proportion of dense garnet and therefore cause a net increase in the density of the mantle column. Even though these effects have long been recognized (e.g., Ringwood, 1975) and are generally accepted by the petrological community, they are rarely taken into account for geodynamic calculations. The standard model that is widely used in geodynamic modeling assumes a solely temperature dependent density (TDD) distribution in the mantle (McKenzie, 1978). This model does not include phase transitions, mantle chemistry, or any pressure dependence of

mantle density and it clearly does not capture the properties and behaviour of the lithosphere during stretching (Petrini et al., 2001; Kaus et al., 2005; Fig. 1). In a realistic mantle, density is non-linear and discontinuous, due to mineral reactions and phase transitions (Green and Ringwood, 1970a,b; Ringwood, 1975; Green and Liebermann, 1976; Podladchikov et al., 1994; Yamasaki and Nakada, 1997; Petrini et al., 2001; Kaus et al., 2005; Fig. 1). In dynamic systems, such as an extending lithosphere, the effect of phase transitions is of major importance and the interplay between changing temperature and mineral reactions can cause large differences in syn- and post-rift basin subsidence (Podladchikov et al., 1994; Yamasaki and Nakada, 1997; Petrini et al., 2001; Kaus et al., 2005). During stretching and basin formation, the lithosphere and the crust thin, and the temperature gradient of the geotherm increases. Phase transitions that take place during basin formation result in discrepancies between the observed subsidence history and the one modeled using TDD (Podladchikov et al., 1994; Yamasaki and Nakada, 1997; Petrini et al., 2001; Kaus et al., 2005). Kaus et al. (2005) described the effect of phase transitions, but used a very restricted range of (oceanic) mantle compositions in their model and did not investigate the geochemical and petrological reasons for the differences in modeled subsidence. In addition, previous studies used either simplified parameterized phase boundaries (Podladchikov et al., 1994; Yamasaki and Nakada, 1997) or based their phase diagram calculations (Petrini et al., 2001; Kaus et al., 2005) on the thermodynamic database of Holland and Powell (1998). This database does not include chromium, which exerts significant

---

* Corresponding author. Tel.: +47 22856922; fax: +47 22855101.
  E-mail address: n.s.c.simon@fys.uio.no (N.S.C. Simon).
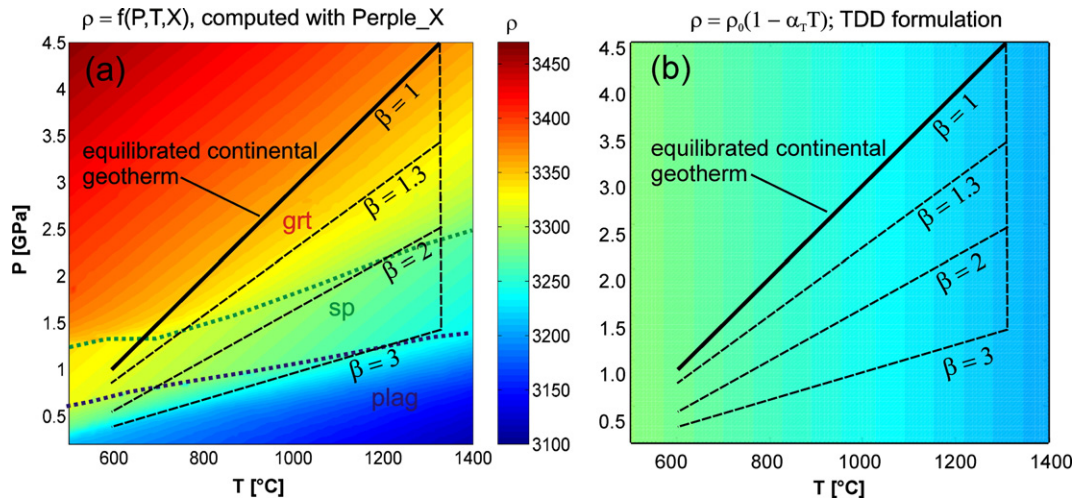
Fig. 1. P–T–ρ diagram calculated with Perple_X for Hawaiian Pyrolite composition given in Table 1 (a) and using the solely temperature dependent (TDD) formulation given by McKenzie (1978; (b)). The two main phase transitions and a series of geotherms for β from 1 to 3 are also shown. Peridotite mantle density slightly increases with temperature along an equilibrated continental geotherm (a), whereas TDD predicts its decrease (b). At constant temperature (in the convecting mantle or asthenosphere), density strongly increases with depth in a peridotite mantle (a). The TDD formulation, however, predicts constant density at constant temperature (b).

control on phase equilibria in the mantle. Chromium has recently been added to the thermodynamic phase diagram calculation program Perple_X (http://www.perplex.ethz.ch), resulting in computed phase diagrams that are in excellent agreement with experimentally derived ones (Fig. 1). In this paper, we explore a wide range of mantle compositions and show how these compositional variations, in conjunction with parameters such as temperature and crustal thickness, affect the density distribution and the mean density of the lithosphere during stretching. We also provide a method to reduce the complex pressure–temperature–composition (P–T–X) dependent density distributions in the mantle to simple parameters that can easily be applied in geodynamic modeling, and will lead to significant improvement of existing models.

2. Methods and results

2.1. The choice of mantle compositions

Studies of mantle xenoliths transported to the surface in alkaline magmas and of mantle peridotites outcropping as ophiolites or peridotite massifs show that the continental upper mantle spans an extremely wide compositional range, from strongly refractory cratonic harzburgites to fertile lherzolites with major element compositions close to those inferred for primitive mantle or "pyrolite" (e.g. recent reviews by Bodinier and Godard, 2003; Pearson et al., 2003). Detailed studies of fossil and recent passive margins and mantle xenoliths from rifts also show that lithospheric stretching is always accompanied by melt infiltration and refertilization of the lithospheric mantle, even at so-called amagmatic margins (e.g., Müntener and Piccardo, 2003), and mantle compositions from rifts and rifted continental margins are often reported as being close to fertile peridotite (for example the Red Sea; Bonatti et al., 1986). In reality, however, passive margin and rift peridotites span the whole range of observed mantle compositions (Pearson et al., 2003). Thus, the effect of compositional variations on mantle densities needs to be understood to model the subsidence of sedimentary basins in an extending lithosphere. Most of the observed compositional range is covered by the compositions selected here. We tested the effect of major element variations (SiO$_2$, MgO, FeO, CaO, Al$_2$O$_3$, Cr$_2$O$_3$, Na$_2$O) on the density effect of phase transitions and found that Al$_2$O$_3$ and Na$_2$O have the most profound effect (further discussed below). We therefore choose to vary only Al$_2$O$_3$ (from 0.5 to 4.5 wt.%) and

Na$_2$O (from 0.05 to 0.45 wt.%) for the detailed density calculations while keeping the other oxide concentrations constant (Table 1). The results are compared with density calculations on natural peridotites from the Ronda massif (Frey et al., 1985) to ensure applicability of the synthetic results to nature. The Ronda peridotites span the whole range from strongly refractory to fertile Proterozoic and Phanerozoic continental mantle (Frey et al., 1985; Table 1). Archaean lithospheric mantle is similar to the most refractory Ronda peridotite in aluminium, sodium and calcium, but distinct in that it has significantly lower iron contents, and in some cases (Kaapvaal, Siberia), significantly higher Si/Mg ratios (e.g., Boyd, 1989), resulting in a lower bulk density of Archaean lithospheric mantle (e.g., Boyd and McCallister, 1976; Poudjom Djomani et al., 2001; Schutt and Lesher, 2006).

The calculations in this paper are simplified in so far as we restricted them to a dry, sub-solidus and closed system mantle. Evaluation of hydration, partial melting and melt infiltration requires quantitative treatment of open system behaviour, including transport, deformation and reaction, which is beyond the scope of this paper. We do, however, provide some speculations on the implications of open system behaviour in the discussion section below.

2.2. Petrology of the upper mantle

Anhydrous peridotite consists of olivine + orthopyroxene + clinopyroxene ± aluminous phase(s) (plagioclase, spinel or garnet), depending on
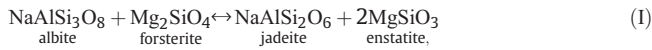
Table 1
Synthetic and natural mantle whole rock compositions used for density calculations

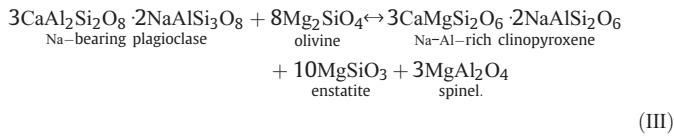| wt.%	Pyrolite synthetic	Ronda (Frey et al., 1985) R893	R347	R25	R243	R123
SiO$_2$	45.20	43.01	44.43	44.43	45.12	45.60
Cr$_2$O$_3$	0.41	0.29	0.34	0.45	0.37	0.31
Al$_2$O$_3$	0.5–4.5	0.89	1.88	2.40	3.64	4.84
FeO(tot)	8.12	7.99	8.12	8.12	8.30	8.80
MgO	37.50	47.17	43.76	42.09	39.09	35.80
CaO	3.08	0.78	1.49	2.61	3.24	4.07
Na$_2$O	0.05–0.45	0.03	0.11	0.16	0.32	0.45
Total		100.16	100.13	100.26	100.08	99.87
Mg#	0.89	0.91	0.91	0.90	0.89	0.88

FeO(tot): total iron as FeO. Pyrolite composition recalculated to 100% for varying aluminum and sodium before phase diagram calculation.

pressure, temperature and composition (Ringwood, 1966; Fig. 1). The following *P–T* dependent phase equilibria control the mineralogy of the uppermost (lithospheric) part of the mantle (Mg^{2+} is interchangeable with Fe^{2+}):

1. Breakdown of plagioclase (from the phase assemblage olivine+ low-Al opx+diopside cpx+plagioclase; Robertson et al., 1957; Kushiro and Yoder, 1966):

$$\underset{\text{albite}}{NaAlSi_3O_8} + \underset{\text{forsterite}}{Mg_2SiO_4} \leftrightarrow \underset{\text{jadeite}}{NaAlSi_2O_6} + \underset{\text{enstatite,}}{2MgSiO_3} \qquad (I)$$

$$\underset{\text{anorthite}}{CaAl_2Si_2O_8} + \underset{\text{forsterite}}{Mg_2SiO_4} \leftrightarrow \underset{\text{Ca–Tschermaks}}{CaAl_2SiO_6} + \underset{\text{enstatite.}}{2MgSiO_3} \qquad (II)$$

The jadeite and Ca-Tschermaks molecule enter into solid solution in pyroxenes that are formed at the expense of plagioclase. The formation of spinel from Na- and Al-bearing plagioclase (Birch and LeComte, 1960; Kushiro, 1965; Green and Ringwood, 1970a,b; Ringwood, 1975) can be written as:

$$\underset{\text{Na–bearing plagioclase}}{3CaAl_2Si_2O_8 \cdot 2NaAlSi_3O_8} + \underset{\text{olivine}}{8Mg_2SiO_4} \leftrightarrow \underset{\text{Na–Al–rich clinopyroxene}}{3CaMgSi_2O_6 \cdot 2NaAlSi_2O_6}$$
$$+ \underset{\text{enstatite}}{10MgSiO_3} + \underset{\text{spinel.}}{3MgAl_2O_4}$$
$$(III)$$

Reaction III is mainly pressure-dependent (slope ~5 bar/°C). In pyrolite, plagioclase appears to be stable to about 1.2 GPa close to the solidus (Ringwood, 1975; Fig. 2b). The exact position of the reactions in *P–T* space is determined by the bulk composition. Na stabilizes plagioclase to higher pressures and the formation of spinel is facilitated in systems with low MgO/FeO ratios and high Cr_2O_3 (Ringwood, 1975; Presnall et al., 2002).

Since the plagioclase-out reaction in mantle peridotite is located at relatively low pressures (25–35 km depth) plagioclase peridotite will not occur as a stable assemblage in cold continents with thick crust. It might be present, however, in areas of high heat flow and thin crust such as mid-oceanic ridges (Ringwood, 1975) and passive margins, where plagioclase peridotite may have a significant influence on lithospheric densities. Formation of plagioclase peridotite in these settings could be responsible for mantle uplift and exhumation. Abundant plagioclase peridotite is reported from the exhumed continental mantle at the Iberian margin (Chazot et al., 2005) and the fossil stretched continental margins in the Alps (Müntener and Piccardo, 2003).

2. Breakdown of spinel (from the assemblage olivine+Al-rich opx+ Al-rich cpx±spinel):

At temperatures close to the solidus, pyroxenes can hold increasing amounts of R_2O_3 ($Al_2O_3+Cr_2O_3+Fe_2O_3$) in solid solution, and spinel decreases with increasing temperature according to the reaction (MacGregor, 1974):

$$\underset{\text{spinel}}{MgAl_2O_4} + \underset{\text{enstatite}}{mMgSiO_3} \leftrightarrow \underset{\text{aluminous enstatite}}{(m-2)MgSiO_3 \cdot MgAl_2SiO_6} + \underset{\text{forsterite.}}{Mg_2SiO_4} \qquad (IV)$$

The extent of the spinel-free olivine+2 pyroxenes field is sensitively dependent upon the R_2O_3/pyroxene ratio of the bulk rock and also upon the Cr/Al ratio of the R_2O_3 component. Experiments on compositions with R_2O_3/pyroxene ratios higher than pyrolite showed an expansion of the spinel+pyroxenes field to higher temperatures, and the spinel-free field close to the solidus seen in experiments on pyrolite was not encountered (Ringwood, 1975; Robinson and Wood, 1998; Klemme and O'Neill, 2000).

At higher pressures, spinel–peridotite becomes unstable and transforms to garnet–peridotite (olivine+low-Al opx+low-Al cpx+
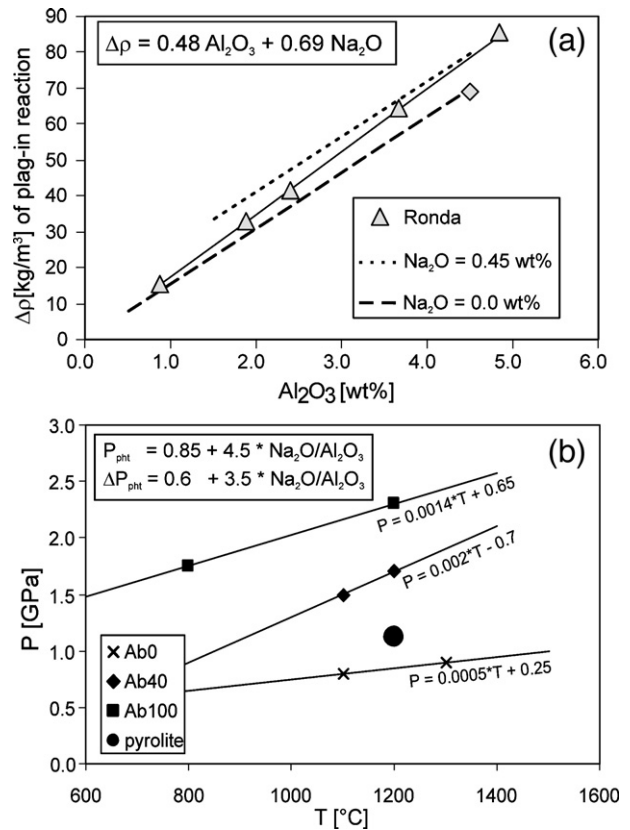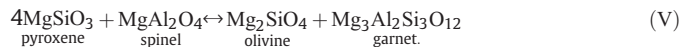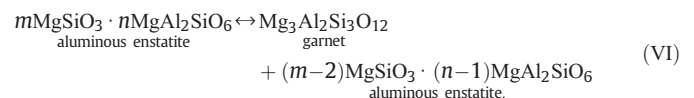

Fig. 2. (a) Whole-rock Al_2O_3 content vs. maximum density change due to formation of plagioclase calculated from the stoichiometry of reaction III, assuming that all aluminium is held in either spinel or plagioclase. Na_2O is kept constant at a minimum (most refractory) and maximum (most fertile) level for the two parallel lines, and co-varies with Al_2O_3 in the Ronda samples (Table 1). The $\Delta\rho$ of the plagioclase-in reaction is dominated by the Al_2O_3 content, which determines how much plagioclase can form in the peridotite, with a minor correction for Na_2O. CaO usually co-varies with Al_2O_3 in natural peridotites and is not a limiting factor. (b) *P–T* diagram showing the Clapeyron slopes of the plagioclase breakdown reaction in simple experimental systems. Pure albite ($NaAlSi_3O_8$) is stable to the highest pressures (2.3 GPa at 1200 °C, reaction I; Robertson et al., 1957), labradorite consisting of 40% albite and 60% anorthite breaks down at around 1.5 GPa (reaction III; Green and Ringwood, 1970a,b) and pure anorthite ($CaAl_2Si_2O_8$) is not stable above 0.85 GPa (reaction II; Kushiro and Yoder, 1966). Breakdown of plagioclase in Hawaiian pyrolite was reported at 1.12 GPa at 1200 °C (Green and Ringwood, 1970a,b). We linearly extrapolated between the experimental data to derive two functions for the pressure of the phase transition, P_{pht} at fixed temperature (1200 °C), and for the slope of the reaction, ΔP_{pht}, as a function of the Na_2O/Al_2O_3 ratio.

pyrope-rich garnet). The spinel–garnet transition can be described by the simplified reaction:

$$\underset{\text{pyroxene}}{4MgSiO_3} + \underset{\text{spinel}}{MgAl_2O_4} \leftrightarrow \underset{\text{olivine}}{Mg_2SiO_4} + \underset{\text{garnet.}}{Mg_3Al_2Si_3O_{12}} \qquad (V)$$

Additional components strongly influence the position of the spinel-out boundary. An increase in Cr_2O_3/Al_2O_3 of the system broadens the spinel stability field and stabilizes spinel to higher and lower pressures (leading to wide fields of co-existing spinel+garnet and spinel+ plagioclase).

The formation of garnet involves two distinct equilibria, and there is a sharp change of gradient where they intersect. The reaction with the shallower slope is reaction (V). Garnet is also formed by the breakdown of aluminous pyroxene according to the (simplified) equilibrium (MacGregor, 1974):

$$\underset{\text{aluminous enstatite}}{mMgSiO_3 \cdot nMgAl_2SiO_6} \leftrightarrow \underset{\text{garnet}}{Mg_3Al_2Si_3O_{12}}$$
$$+ \underset{\text{aluminous enstatite.}}{(m-2)MgSiO_3 \cdot (n-1)MgAl_2SiO_6}$$
$$(VI)$$

An analogous reaction can be written for aluminous diopside. The solid solution of garnet in pyroxene decreases with increasing pressure and decreasing temperature.

Kaus et al. (2005) have shown that the plagioclase–spinel transition is the most important phase transition during stretching since it has the highest density difference. Phase transitions in the crust have negligible influence on basin subsidence in the stretched lithosphere (Kaus et al., 2005). We therefore ignore crustal phase transitions and assume constant crustal densities. The focus in this contribution is on the plagioclase–spinel transition, and we put less emphasis on the garnet–spinel transition (which is, however, included in the phase diagram and density calculations below).

2.3. Simplified calculations: mineral end member reactions, $\Delta\rho$ and depth of plagioclase-in reaction

Reaction (III) takes place at about 1.5 GPa at 1100 °C and 1.7 GPa at 1200 °C (Green and Ringwood, 1970a,b) and the density increase of the reaction, $\Delta\rho_{plag\text{-}sp}$, is 377 kg/m^3, calculated from stoichiometric relationships and the molar volumes of the minerals. For a natural peridotite composition, the amount of plagioclase that can be formed is generally restricted by the amount of Al_2O_3 and Na_2O in the bulk. If we ignore the solubility of aluminium in pyroxenes and use all available Al_2O_3 to make plagioclase we can calculate the maximum amount of plagioclase that can form at a given Al_2O_3 concentration in the bulk rock (Fig. 2a). Usually peridotite has a very high Ca/Na ratio hence Ca is not a limiting factor. For a given Al_2O_3 content in the bulk rock, however, the total amount of plagioclase increases with increasing Na_2O since one mole of albite ($NaAlSi_3O_8$) contains less Al_2O_3 than one mole of anorthite ($CaAl_2Si_2O_8$). After calculating the amount of plagioclase as a function of the bulk rock Al_2O_3 and Na_2O contents the $\Delta\rho_{plag\text{-}sp}$ can be derived as a function of whole rock Al_2O_3 and Na_2O from the simplified linear equation $\Delta\rho_{plag\text{-}sp}$ [wt.%] = 0.48 Al_2O_3 [wt.%] + 0.69 Na_2O [wt.%]. Application of this equation to natural peridotites leads to $\Delta\rho_{plag\text{-}sp}$ smaller than 10 kg/m^3 for extremely refractory compositions and up to 90 kg/m^3 (~3%) for fertile or primitive mantle compositions (Fig. 2a).

The depth of the spinel–plagioclase phase transition also depends strongly on composition because the sodium end-member albite (Ab100, Fig. 2b) is stable to higher pressures (2.3 GPa at 1200 °C; Robertson et al., 1957) than the calcium end-member anorthite (Ab0, Fig. 2b; 0.85 GPa at 1200 °C; Kushiro and Yoder, 1966). The positions of the plagioclase–spinel transitions for the two end-member reactions (Eqs. (I) and (II), Ab100 and Ab0, respectively), an intermediate plagioclase (Ab40, Eq. (3)) and pyrolite (Robertson et al., 1957; Birch and LeComte, 1960; Kushiro, 1965; Kushiro and Yoder, 1966; Green and Ringwood, 1970a,b) are shown in P–T space in Fig. 2b. The pressures of the phase transitions at a fixed temperature (1200 °C), P_{pht}, and the slope of the plagioclase–spinel phase transitions, expressed as ΔP_{pht} between 0 and 1200 °C, depend on the Na_2O/Al_2O_3 ratio and can be approximated by linear expressions: $P_{pht} = 8.5 + 45 \cdot Na_2O/Al_2O_3$ and $\Delta P_{pht} = 6 + 35 \cdot Na_2O/Al_2O_3$. These simplified relationships are only valid for reasonable Na_2O/Al_2O_3 in the bulk rock (<0.3) and produce erroneous results for higher Na_2O/Al_2O_3.

These calculations are consistent with the experimentally determined positions of the plagioclase-out boundaries and their dependence on composition (Presnall et al., 2002). These authors also note that adding iron to the CMAS system has an effect similar to adding sodium and stabilizes plagioclase to higher pressures. Spinel co-exists with plagioclase at low pressures in the more complex systems (Presnall et al., 2002), in agreement with our full thermodynamic calculations.

The position and slope of the garnet–spinel transition for different bulk compositions have been intensely investigated experimentally since the 1960s (Green and Ringwood, 1967; O'Neill, 1981; Robinson and Wood, 1998; Brey et al., 1999; Klemme and O'Neill, 2000; Walter et al., 2002 and references therein). The exact location and shape of

this phase transition has been debated, especially at low temperatures (Walter et al., 2002 and references therein; Wood and Yuen, 1983). Phase diagram calculations using the new Perple_X include thermodynamic data and solid solution models for chromium end members and are consistent with experimental results from most simple and complex systems (Green and Ringwood, 1967; Robinson and Wood, 1998) and theoretical predictions using the currently available thermodynamic data for mineral end members and solution models.

### 2.4. Effect of other elements on bulk density vs. phase transition effects

Previous studies on the influence of mantle composition on density (Poudjom Djomani et al., 2001; Schutt and Lesher, 2006) emphasized the effect of Mg# (Mg/(Mg + Fe)), which increases during partial melting of peridotite. Whereas the Mg# of a peridotite has a strong effect on the bulk density of the mantle, it has little effect on phase transitions. It therefore does not influence the magnitude of the density changes that occur during active deformation (thinning) of the lithosphere. We therefore choose to keep FeO and MgO and all other components constant while varying Al_2O_3 and Na_2O in the Perple_X phase diagram calculations. This procedure is justified by comparison with the Ronda peridotites. Mg# in the latter varies from 87.9 to 91.3, encompassing the range from fertile to relatively refractory mantle (Frey et al., 1985). The calculated initial mean density (ρ_1) at $\beta = 1$ ($\beta = z_{lith(1)}/z_{lith(\beta)}$, see Table 2 for a definition of all parameters) of the lithospheric column from the surface to a compensation depth of 150 km ($z_{crust(1)} = 35$ km, constant $\rho_{crust} = 2900$ kg/m^3) ranges from 3260 kg/m^3 for the most fertile (lowest Mg#, highest Al) composition to 3211 kg/m^3 for the most refractory (highest Mg#, lowest Al) Ronda composition, compared to 3249 kg/m^3 and 3219 kg/m^3 for the most fertile (highest Al and Na) and most refractory (lowest Al and Na, all other elements constant) synthetic compositions, respectively. The greater range in ρ_1 of the Ronda samples reflects the effect of changes in Mg# on the absolute density, that add on to the effect of Al_2O_3.

2.5. One-dimensional geometric relationships

Stretching of the lithosphere, the evolution of the geotherm and the resulting changing depth of the phase boundary in the lithospheric column are schematically illustrated in Fig. 3. We followed the approach of McKenzie (1978) for lithospheric stretching, but added one phase transition (see Podladchikov et al., 1994; Yamasaki and

Table 2
Description and values of parameters used in the calculations

Symbol	Description	Values	Unit
Parameter variation for dimensional analysis			
T	Temperature		°C
P	Pressure		Pa
$z_{pht(Tast)}$	Depth of plag-in reaction at T_{ast}	$32*10^3$–$54*10^3$	m
z_r	Intersection of the geotherm and the phase transition		m
α	Slope of initial geotherm	0.005–0.013	°C/m
γ	Slope of the plag-in reaction	0.023–0.064	°C/m
C	Crust/lithosphere thickness ratio	0.1–0.5	
R	Geotherm/slope of pht (α/γ)	0.1–0.5	
D	$z_{pht(Tast)}/z_{lith1}$	0.16–0.68	
Parameters used for stretching calculations			
$z_{crust(1)}$	Initial crustal thickness at $\beta = 1$	$35*10^3$	m
$z_{lith(1)}$	Initial lithosphere thickness at $\beta = 1$	$150*10^3$	m
β	Stretching factor, $z_{lith(1)}/z_{lith(\beta)}$		
T_{ast}	Temperature of asthenosphere	1330	°C
T_{MOHO}	Temperature at crust–mantle	600	°C
ρ_0	Mantle density at 0 °C for TDD	3330	kg/m^3
ρ_{crust}	Density of crust	2900	kg/m^3
α_T	Thermal expansion coefficient	$3.28*10^{-5}$	K^{-1}
β_P	Compressibility	Not used	
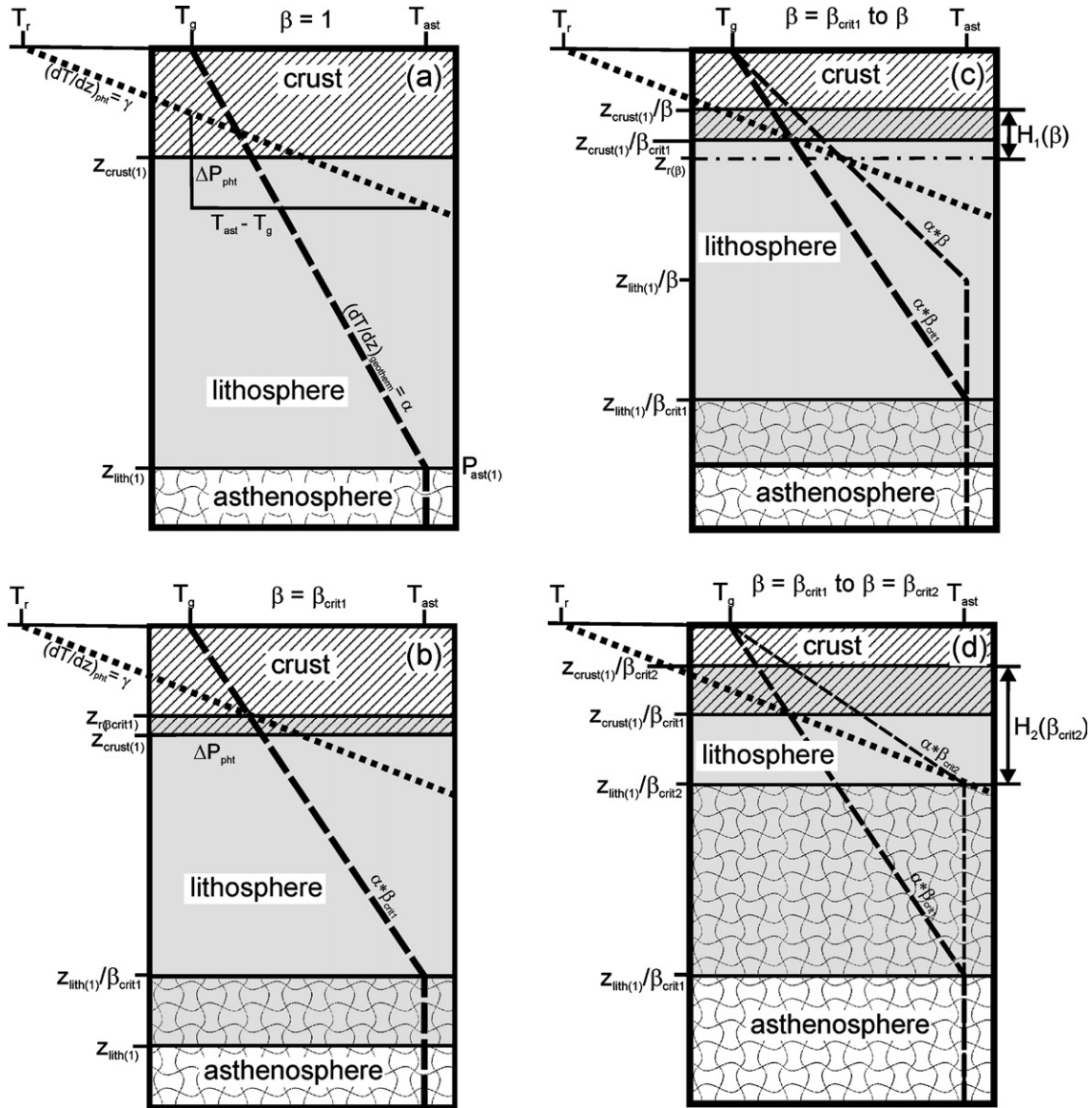
Fig. 3. Schematic drawing showing the geometric relationships between a phase transition and an evolving geotherm during lithospheric thinning. Heavy dotted line: phase transition; dashed lines: geotherms; solid lines: base of the lithosphere and base of the crust. (a): Initial conditions ($\beta=1$); (b): Thinning up to β_{crit1}, where the intersection between the phase transition and the geotherm (z_r) coincides with the base of the crust. (c): Thinning from β_{crit1} to an arbitrary β between β_{crit1} and β_{crit2}. H_1 denotes the length of the column that is in the plagioclase stability field. (d): Thinning from β_{crit1} to β_{crit2}, where the phase transition intersects the adiabatic part of the geotherm at T_{ast} (the base of the lithosphere). H_2 will grow upwards with continued thinning of the crust. See text for explanation.

Nakada, 1997 for a similar approach). This model assumes that stretching is instantaneous and homogeneous throughout the crust and mantle. Instantaneous stretching implies that stretching (advection of hot material) is fast compared to cooling (thermal diffusion), so thermal re-equilibration by diffusion can be neglected. Changes in the column are considered from a constant compensation depth at $z_{lith(1)}$ to the top of the crust. Only the spinel–plagioclase–peridotite phase transition is shown in Fig. 3 since the garnet–spinel–peridotite phase transition has been investigated in a similar way before (Podladchikov et al., 1994) and has a much smaller effect on basin subsidence/uplift (Petrini et al., 2001; Kaus et al., 2005). The spinel–plagioclase phase transition has a small positive slope at relevant mantle temperatures and compositions (e.g. Ringwood, 1975; Presnall et al., 2002).

The geotherm can be described with the equation

$$T = T_g + \alpha \cdot z, \tag{1}$$

where T is temperature [°C], z is depth [m], $\alpha=dT/dz$ is the slope of the geotherm and T_g is the intersection of the extrapolated mantle geotherm with the surface ($z=0$).

The phase transition can be approximated by the linear expression

$$T = T_r + \gamma \cdot z \tag{2}$$

with $\gamma=dT/dz$ the slope of the phase transition and T_r the extrapolated temperature at $z=0$, where the Clapeyron slope would intersect the surface.

In the starting configuration, the equilibrated geotherm misses the spinel–plagioclase transition because the intersection between the geotherm and the Clapeyron slope of the reaction, z_r, is located inside the crust: $z_r < z_{crust}$ (Fig. 3a). After stretching and thinning of the lithospheric mantle and crust by a critical factor β_{crit1}, the slope of the geotherm increases and the intersection with the Clapeyron slope of the reaction, z_r, has moved deeper and is now located at the base of

the crust ($z_r = z_{crust(1)}/\beta_{crit1}$). With progressive stretching, part of the column with length H_1 moves into the plagioclase stability field. Further stretching leads to increasing H until a critical stretching factor β_{crit2} is reached and z_r coincides with the base of the lithosphere ($z_r = z_{lith(1)}/\beta_{crit2}$). During further stretching z_r stays constant and the increase of plagioclase peridotite in the column (H_2) is caused only by the continued thinning of the crust. The critical stretching factors, β_{crit1} and β_{crit2}, and the lengths of the column that are in the plagioclase stability field, H_1 and H_2, can be calculated by introducing three dimensionless numbers.

The ratio of the slope of the initial geotherm:

$$\alpha = \left(\frac{dT}{dz}\right)_{geo} = \frac{T_{ast} - T_g}{z_{lith(1)}} \tag{3}$$

and the slope of the phase transition (inverse Clapeyron slope):

$$\gamma = \left(\frac{dT}{dz}\right)_{pht} = \frac{T_{ast} - T_r}{z_{pht(T_{ast})}} \tag{4}$$

give the first dimensionless number:

$$R = \frac{\alpha}{\gamma} = \frac{T_{ast} - T_g}{T_{ast} - T_r} \cdot \frac{z_{pht(T_{ast})}}{z_{lith(1)}} = \frac{\Delta P_{pht}}{P_{ast(1)}}. \tag{5}$$

Note that γ stays constant during stretching for a given bulk rock composition whereas α changes with stretching: $\alpha = \alpha_1 \cdot \beta$.

The second number is the ratio of the thickness of the crust to the total lithospheric thickness and is frequently used in basin modeling:

$$C = \frac{z_{crust}}{z_{lith}}. \tag{6}$$

The third number is the ratio of the depth of the phase transition at T_{ast} to the thickness of the lithosphere:

$$D = \frac{z_{pht(T_{ast})}}{z_{lith(1)}}. \tag{7}$$

The critical points in this thinning process may now be expressed as follows. The depth of the reaction, z_r, can be calculated from the intersection between the geotherm and the phase transition. At β_{crit1}

$$z_r = \frac{T_g - T_r}{\gamma - \alpha\beta_{crit1}} = \frac{z_{crust(1)}}{\beta_{crit1}}, \tag{8}$$

therefore

$$\beta_{crit1} = \frac{z_{crust(1)} \cdot \gamma}{T_g - T_r + z_{crust(1)} \cdot \alpha} = \frac{C}{D + R(C - 1)} \tag{9}$$

and

$$H_1 = \frac{T_g - T_r}{\gamma - \alpha\beta} - \frac{z_{crust(1)}}{\beta} = \frac{\gamma z_{pht(T_{ast})} - \alpha z_{lith(1)}}{\gamma - \alpha\beta} - \frac{z_{crust(1)}}{\beta}$$
$$= z_{lith(1)}\left(\frac{D - R}{1 - R\beta} - \frac{C}{\beta}\right). \tag{10}$$

The second critical stretching factor is reached when z_r coincides with $z_{crust(1)}/\beta_{crit2}$ and $T(z_r) = T_{ast}$, so that

$$\beta_{crit2} = \frac{\gamma z_{lith(1)}}{T_g - T_r + \alpha z_{lith(1)}} = \frac{z_{lith(1)}}{z_{pht(T_{ast})}} = \frac{1}{D} \tag{11}$$

and

$$H_2 = \frac{z_{lith(1)}}{\beta_{crit2}} - \frac{z_{crust(1)}}{\beta} = z_{lith(1)}\left(\frac{1}{\beta_{crit2}} - \frac{C}{\beta}\right). \tag{12}$$

The fraction of the lithosphere that is in the plagioclase field ($H/z_{lith(1)}$) increases rapidly between β_{crit1} and β_{crit2} and only moderately for

$\beta > \beta_{crit2}$ (Fig. 4). Hence H at β_{crit2} is close to the maximum fraction of plagioclase peridotite that can be reached during stretching, and β_{crit2} marks this saturation point. At β_{crit1}, $H = H_1 = 0$ and at β_{crit2}, $H_1 = H_2$. Fig. 4 shows the dependence of H, β_{crit1} and β_{crit2} on β and C for average D and R values (Table 2). β_{crit1} is <1 for low crust/lithosphere ratios (0.1) and increases to 2.5 if the initial crust constitutes half of the lithosphere. β_{crit2} is constant at 3.3, where H can reach 25% for small crust/lithosphere ratios. H is largest for large D and R and small C and can reach a maximum of 0.57 within the parameter range assumed here (Table 2). β_{crit1} decreases with D and increases with R and C, while β_{crit2} is independent of R and C and decreases with D.

2.6. Full thermodynamic calculation of density

The Gibbs free energy minimization software Perple_X (Connolly and Petrini, 2002) was used to calculate phase diagrams for a range of mantle compositions (see supplementary data in the Appendix). At any point in P–T space, Perple_X gives the proportions and compositions of all stable phases. From there, thermodynamic P–T–X dependent densities can be obtained without any extrapolation. All following diagrams are computed assuming an initial lithospheric thickness $z_{lith(1)} = 150$ km, initial crustal thickness $z_{crust(1)} = 35$ km, $T_{ast} = 1330$ °C, $T_{MOHO} = 600$ °C and a constant $\rho_{crust} = 2900$ kg/m^3. To calculate mean densities or weights of the columns, densities are integrated from $z_{lith(1)}$ to the top of the crust. Stretching and thinning are assumed to be instantaneous in these simple models. As shown above (Fig. 1), mantle mineralogy results in non-linear density variations, and large density contrasts may occur at some phase boundaries (Fig. 5). These contrasts are most pronounced for a fertile mantle since the amount of aluminous phases that can be formed is a function of Al_2O_3 in the bulk-rock (Wood and Yuen, 1983). Whole-rock Na_2O content determines the position of the plagioclase-in boundary. For a very refractory mantle, density can be approximated by the simple P–T dependent formula $\rho = \rho_0(1 - \alpha_T T + \beta_P P)$. However, the pressure dependence of ρ is as strong as the temperature dependence (lower left corner in Fig. 5), and the effect of compressibility (β_P) cannot be neglected.

2.7. Density along the geotherm and the effect of stretching

The hydrostatic pressure in the lithospheric column is determined by the load of the overburden, while the temperature distribution is given by the geothermal gradient. The equilibrated, steady state mantle geotherm is well approximated by a linear function with a slope $\alpha = dT/dz$
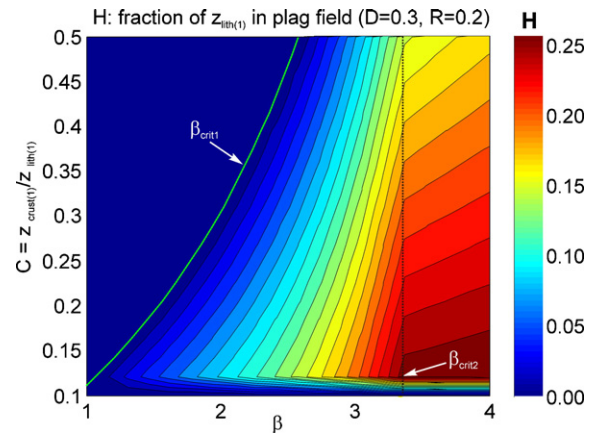

Fig. 4. $H/z_{lith(1)}$ as a function of β and the initial ratio of crustal and lithospheric thicknesses, C. D and R are kept constant. At $\beta > \beta_{crit1}$, the lithospheric mantle first enters the plagioclase stability field ($H/z_{lith(1)} = 0$). $H/z_{lith(1)}$ then increases almost linearly up to $\beta = \beta_{crit2}$. At $\beta > \beta_{crit2}$, the depth of the phase transition coincides with the depth of the stretched lithosphere and $H/z_{lith(1)}$ increases only slightly due to continued thinning of the crust. β_{crit1} increases with increasing C (Eq. (9)), whereas β_{crit2} only depends on D and is constant for fixed D. Up to 25% of the initial lithosphere can be in the plagioclase field for small C and large β.
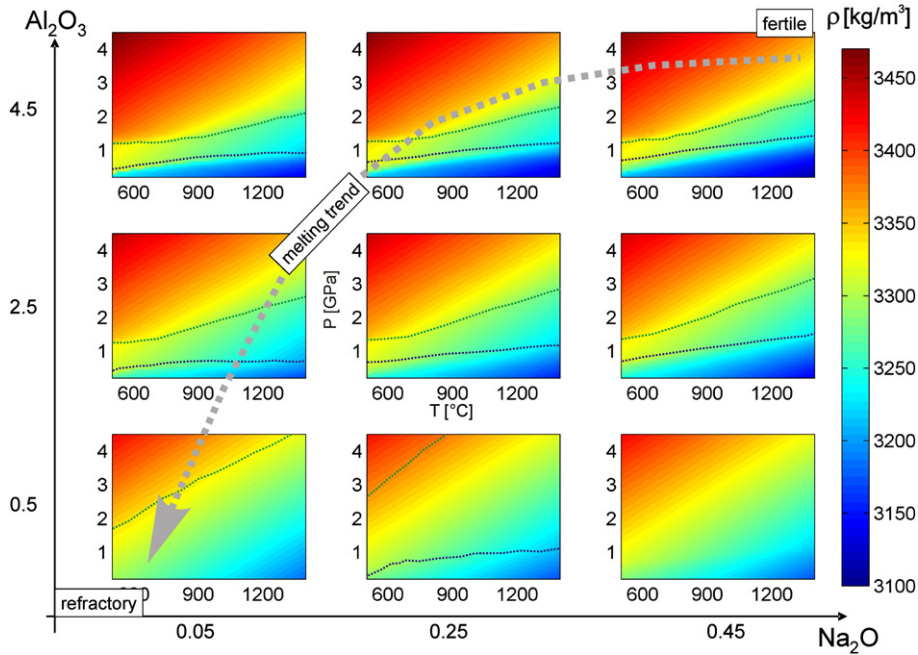
Fig. 5. Variation of mantle density as a function of pressure, P, and temperature, T, (inner axes) and composition, X, (outer axes). Mantle density depends on pressure and temperature and is discontinuous in P–T space due to phase transitions. Plagioclase peridotite is stable below the dark blue dotted line, the spinel field roughly coincides with the green, intermediate density, colours, whereas dense garnet peridotite appears in orange-red shading above the green dotted line. The density contrast in P–T space decreases with decreasing Al_2O_3 (from top to bottom), whereas the extent of the plagioclase field increases with increasing Na_2O (from left to right).

connecting the base of the lithosphere z_{lith} with a temperature T_{ast} and the base of the crust z_{crust} with a temperature T_{MOHO}. During stretching, the lithosphere and the crust thin, and the temperature gradient of the geotherm increases (Figs. 1 and 3). Table 2 lists the parameters used in our simplified stretching calculations. A geotherm for a thermally equili-

brated 150 km thick continental lithosphere and reference geotherms for variably stretched lithosphere are plotted in Fig. 1a. Densities depending only on thermal expansion (TDD) are shown for comparison in Fig. 1b. Peridotite mantle density slightly increases with temperature along an equilibrated continental geotherm, whereas TDD predicts its decrease. At
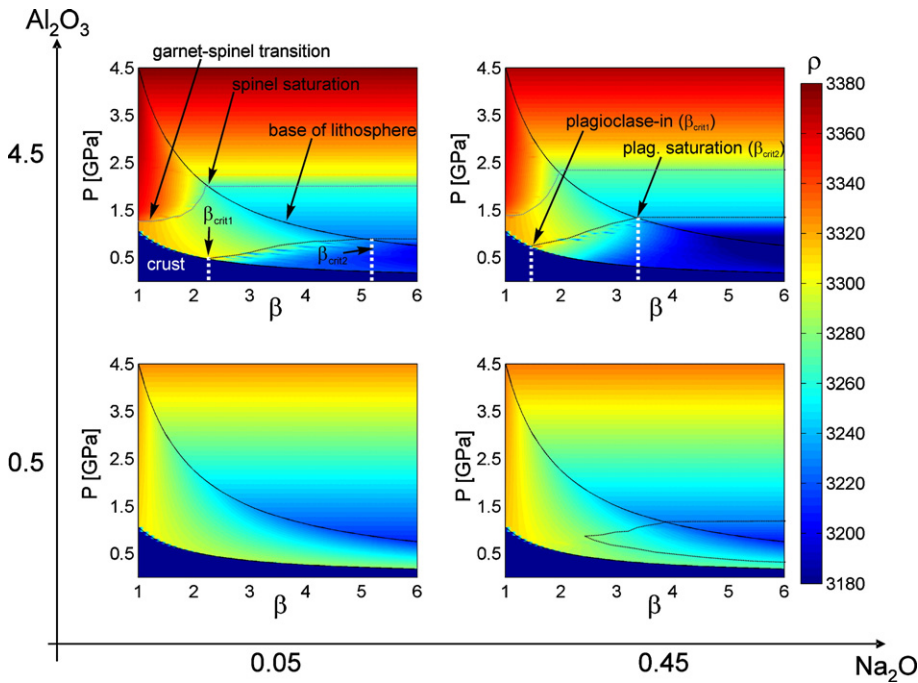
Fig. 6. Density along the geotherm (T projected to P) as a function of stretching, β, and composition. The black solid line indicates the bottom of the lithosphere (1330 °C). In general, density decreases with decreasing pressure along the geotherm, also at constant temperature (below the base of the lithosphere). From the bottom to the top of the column, abrupt reductions in density occur at the garnet-out boundary (~1%), at the plagioclase-in boundary (up to 3%) and at the crust–mantle boundary. Note that the garnet-out boundary (blue thin stippled line) drastically shifts to deeper levels (from ~1.5 to 2.5 GPa) at the initial stages of rifting. Plagioclase–peridotite (below black thin stippled line) first appears in the column between $\beta=1.4$ and $\beta=2$ (β_{crit1}: intersection of the base of the crust with the plag-in transition) at <1 GPa. Its proportion in the column (H) gradually increases until the column becomes saturated in plagioclase–peridotite at β_{crit2} (~3.2 for fertile mantle). β_{crit1}, β_{crit2} and H depend on the initial setup of the lithosphere and the composition of the mantle. The variation in density along the geotherm and the effect of phase transitions on density is most pronounced for fertile compositions (upper right corner).

constant temperature (in the convecting mantle or asthenosphere), density strongly increases with depth in a peridotite mantle. The TDD formulation, however, predicts constant density at constant temperature.

Fig. 6 shows how the distribution of density with depth, projected on the geotherm, changes with increasing stretching (β) and with changing concentrations of Na_2O and Al_2O_3. The density contrast along the geotherm and the depth of the plagioclase-in transition (blue low density field in Fig. 6) clearly increase with increasing fertility (increasing Na_2O and Al_2O_3) of the whole-rock. For the most fertile compositions, plagioclase peridotite appears in the column at ~0.7 GPa and β_{crit1} ~ 1.5. The column becomes saturated in plagioclase at β_{crit2} ~ 3.5, and a significant portion of the column (from a depth corresponding to 1.3 GPa to the base of the thinned crust, i.e. $H > 30$ km) consists of light plagioclase peridotite.

The garnet–spinel phase transition rapidly shifts to deeper depth with increasing stretching due to the steep and curved slope of the phase boundary (Podladchikov et al., 1994), from ~1.4 GPa at $\beta = 1$ to 2.3 GPa at $\beta = 1.9$ in Hawaiian pyrolite (Fig. 6, upper right panel). After the base of the lithosphere has intersected the phase transition the column is saturated in spinel peridotite and the mean density of the mantle part of the lithospheric column has decreased by 1.4% (from $\beta = 1$ to $\beta = 2$).

The change in the mean density of the column ($\bar{\rho}_{\beta=1} - \bar{\rho}_\beta$), which determines the isostatic equilibrium and therefore the subsidence or uplift in the developing basin, is strongly influenced by phase transitions (Fig. 7). In the initial stages of stretching column weights calculated with Perple_X and TDD increase due to thinning of light crust. For relatively fertile compositions, the density increase of the column is reduced by the garnet–spinel transition between $\beta = 1.5–2$ (Fig. 7). The most drastic reduction in peridotite density occurs as soon as sufficient plagioclase peridotite forms in the column at around $\beta = 2.5$. At $\beta > 3.5$, the TDD formulation overestimates the mean density increase by up to 100% for fertile compositions for this particular setup. The difference between TDD and petrologic density decreases for less dense and/or thicker crust, and dramatically increases for denser and/or thinner crust. Since the changes in mean column densities are proportional to subsidence this difference translates into more than 1000 m less subsidence for fertile compositions (e.g. R123, Table 1) calculated with Perple_X relative to TDD at $\beta = 4$ (Fig. 7). TDD approximates true densities and subsidence for
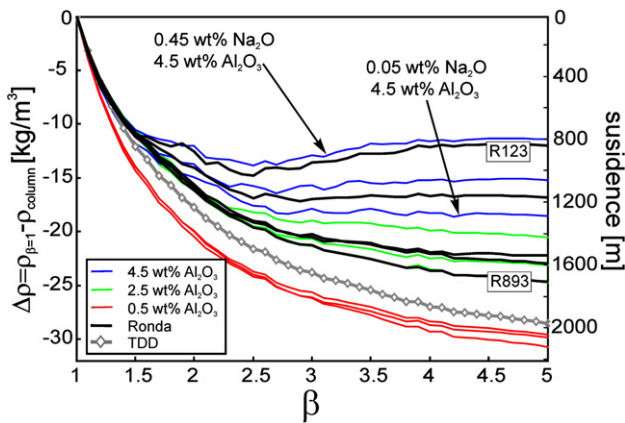
the strongly refractory synthetic mantle compositions used here, but note that the most refractory natural composition (R893, Table 1) still shows ~300 m less subsidence than TDD for large stretching. This is because the most depleted Ronda sample is less refractory than the most extreme model examples (min. Al_2O_3 for Ronda = 0.89 wt.%, vs. 0.5 wt.% in the model compositions; Table 1) and because the effect of depletion on for example Fe is also taken into account. The calculations using the Ronda compositions should more adequately predict density variations in nature than the model compositions since Na and Al co-vary with other elements (e.g. Mg, Fe, Ca) along melting/refertilization trends.

3. Discussion and implications

3.1. Comparison between complex and simplified calculations

Our results have confirmed previous suggestions that phase transitions influence density in areas of thin crust and elevated heat flow (Ringwood, 1975; Podladchikov et al., 1994). We concur with previous findings (Petrini et al., 2001; Kaus et al., 2005) that phase transitions can cause significant synrift uplift and a subsidence curve that is very different to the one modeled by uniform stretching using TDD (i.e., less synrift subsidence or synrift uplift followed by accelerated subsidence; Fig. 7). We have also investigated and quantified the effect of changes in mantle composition, first from simplified petrological considerations using end member reactions and geometrical relationships between phase boundaries, geotherms and crust and lithosphere thicknesses; then from full thermodynamic calculations for a range of synthetic and real mantle compositions. The full thermodynamic calculations of density agree well with the simplified calculations based on end member reactions, which predict a maximum decrease in column density of 20 kg/m^3 at $\beta = 4$, slightly higher than the Perple_X calculations (Fig. 7; see supplementary data for a more detailed comparison). The Perple_X calculations are also consistent with experimentally derived mantle phase diagrams for simple and complex systems (Ringwood, 1975; Robinson and Wood, 1998; Presnall et al., 2002; Girnis et al., 2003; Klemme, 2004). The calculations of $\Delta\rho$, z_{pht}, critical β's and H from the simplified end member relations and the full thermodynamic calculations give very similar results and predict that subsidence may be reduced by >1000 m for fertile mantle relative to refractory mantle and TDD (Fig. 7 and supplementary material). The simplified calculations consider variations in z_{crust}/z_{lith} and the slope of the geotherm, while the full thermodynamic calculation were carried out with fixed starting geometry and quantify the effect of changes in mantle compositions. Since we used the same parameters as McKenzie (1978) for one dimensional stretching the results can be directly compared to most basin models without phase transitions. Our results can be easily implemented into more complex dynamic or kinematic basin models (Podladchikov et al., 2006; Hartz et al., 2007).

3.2. Reaction kinetics and closed vs. open system behaviour

The importance of phase transitions has often been doubted because of concerns about kinetics. In fact, many metamorphic reactions are sluggish and do not proceed at low temperatures. However, we have shown in the previous sections that the effect of mantle phase transitions on basin subsidence is most pronounced at high stretching factors, implying significant upwelling of hot (>1000 °C) mantle. We therefore assume that reaction kinetics do not inhibit phase transitions in extensional settings. This conclusion is supported by the fact that plagioclase peridotite is frequently observed in shallow mantle peridotites (Dick and Bullen, 1984; Müntener and Piccardo, 2003; Chazot et al., 2005). A large proportion of this plagioclase probably crystallized from infiltrating fluids/melts (Dick and Bullen, 1984; Müntener and Piccardo, 2003; Chazot et al., 2005) as opposed to being formed by closed system metamorphic reactions, but the exact origin

Fig. 7. (a) Variations in column weight ($\bar{\rho}_{\beta=1} - \bar{\rho}_\beta$) calculated for $P–T–X$ dependent densities compared to TDD (grey diamonds). The fields of equal Al_2O_3 contents are bounded by the lowest (lower bound) and highest (upper bound) Na_2O at a given Al_2O_3. All weights are calculated from 150 km ($z_{lith(1)}$) to the top of the crust, assuming a constant crustal density of 2900 kg/m^3 and initial crustal thickness $z_{crust(1)} = 35$ km. Water-loaded tectonic subsidence is proportional to the change in column weight. TDD approximates the density evolution of strongly refractory mantle. For fertile peridotite, TDD overestimates the increase in column weight by more than 100% at $\beta = 4$ and predicts 1800 m of subsidence, compared to 800 m for the most fertile synthetic or Ronda composition (R123). The column weights calculated for the Ronda peridotite compositions (black solid lines) are consistent with the trends displayed by the synthetic compositions.

of the plagioclase is irrelevant for our conclusions. Detailed field work on fossil and current passive margins has confirmed that lithosphere extension is inevitably accompanied by extensive infiltration of the stretched lithospheric mantle by magmatic fluids (Müntener and Piccardo, 2003; Chazot et al., 2005). This leads to re-fertilization of the mantle, direct crystallization of new plagioclase and formation of plagioclase at the expense of spinel. The metamorphic reaction is enhanced by the flux provided by the infiltrating melts, shifting metamorphic closure temperatures to lower values. Open system behaviour should therefore enhance the effect of the plagioclase phase transition. Refertilization of the mantle might also happen independently of extension. If a static mantle is pervasively fluxed by fluids to an extent that the bulk composition changes (e.g. Na and Al increase due to reaction of a basaltic melt with a harzburgite) this will lead to changes in density enhanced by shifting phase boundaries. Alternatively, partial melting of the lithosphere leaves a more refractory peridotite with a more uniform density distribution and a lower average density (Figs. 5 and 6). In either case vertical movements independent of tectonic activity and deformation will occur.

3.3. Implications for geodynamics

We have shown that mantle phase transitions are responsible for a non-linear density distribution in the mantle lithosphere and that their influence on density evolution during stretching depends on mantle composition. The garnet–spinel transition plays an important role during initial stages of rifting (small β) and can cause early syn-rift uplift (probably often interpreted as pre-rift), followed by accelerated subsidence. This is in general accordance with previous work (Podladchikov et al., 1994; Yamasaki and Nakada, 1997; Petrini et al., 2001; Kaus et al., 2005), but our improved phase diagram calculations yield garnet–spinel peridotite boundaries that are more consistent with experimental data and field observation, and constrain systematic variations with changing bulk composition (varying fertility or melt depletion) of the mantle. The spinel–plagioclase transition, in contrast, is important in regions of thin crust and high heat flow (large β), and should therefore play an important role at for example strongly extended continental margins. There, its effect on density can be on the same order of magnitude as the effect of thermal expansion. This means that the reduction in density due to a large proportion of plagioclase in the mantle is equivalent to heating by >500 °C if the conventional solely temperature dependent formulation (TDD) is used to calculate mantle densities. Uplift due to mantle phase transitions is expected to be most pronounced for dense and/or thin initial crust.

We therefore propose that the density reduction due to the formation of plagioclase peridotite might provide an alternative explanation for uplift events that are most commonly explained by processes involving massive heating, either through impingement of a plume (dynamic and thermal uplift) or strong thinning of the mantle relative to the crust (depth dependent stretching). Both these scenarios should be accompanied by elevated paleo-heat flow and probably extensive magmatism.

Perhaps one of the best documented cases of syn-rift uplift in an extended continental margin is the Vøring Plateau, which formed during the ~65–55 Ma pre-break-up rifting episode of the North Atlantic, off-shore Western Norway (e.g. Ren et al., 2003). Preliminary two-dimensional modeling using Tecmod (Rüpke et al., 2007) has shown that the basin evolution of the Vøring basin, including paleo-heat flow and paleo-water depth, can be successfully fitted if differential stretching of the mantle is permitted (Podladchikov et al., 2006; Simon et al., 2007). The necessary mantle stretching can be reduced significantly from the extremely high values required by the conventional TDD formulation to realistic values if petrological density maps are used instead (Podladchikov et al., 2006; Simon et al., 2007). Detailed results of the application of our results to kinetic two-dimensional forward modeling (Rüpke et al., 2007) of the profile from the Vøring Basin will be presented elsewhere.

In dynamic models that explore the transition from passive to active rifting (Huismans et al., 2001) we would expect the plagioclase-in reaction to enhance the active upwelling of the mantle. The interplay between passive stretching (far field tectonic stresses), active mantle upwelling (temperature-induced buoyancy), partial melting and re-fertilization of overlying mantle (compositional changes), and metamorphic phase changes might potentially explain a range of observations at increasingly well studied current and fossil passive margins. The dynamic coupling of these processes provides an interesting field for future research.

Another case where strong uplift is often observed is the so-called 'break-up unconformity' at rifted continental margins, initially interpreted to occur at the transition from rifting to seafloor spreading (Falvey, 1974). However, a similar unconformity is reported from failed intra-continental rifts, where the unconformity is located at the boundary between syn- and post-rift sediments (Ziegler and Cloetingh, 2004). Braun and Beaumont (1989) explained the break-up unconformity by flexural response of the lithosphere to changes in the in-plane stresses, which would be largest during lithospheric rupture. We have shown that the formation of plagioclase peridotite can cause significant buoyancy and therefore uplift in strongly extended lithosphere. This effect will be amplified by re-fertilization of the mantle due to infiltration of melts at the onset of magmatism shortly before break-up. Whitmarsh et al. (2001) have documented the increase in magmatic infiltration of the stretched lithospheric mantle from the continental part of the Iberian and fossil Alpine margins towards the rift centre/break-up location. We therefore propose that uplift at the transition from rifting to sea-floor spreading could be caused by mantle phase transitions. Formation of plagioclase peridotite demonstrably happens in such settings and we have shown here that it is a powerful mechanism for vertical motions in a smoothly extending lithosphere, without invoking sudden changes in temperature or stress. The exact magnitude of the uplift and the interaction with other mechanical and thermal processes needs to be explored in more sophisticated dynamic models.

Appendix A. Supplementary data

Supplementary data associated with this article can be found, in the online version, at doi:10.1016/j.epsl.2008.04.027.

References

Birch, F., LeComte, P., 1960. Temperature–pressure plane for albite composition. Am. J. Sci. 258, 209–217.

Bodinier, J.L., Godard, M., 2003. Orogenic, ophiolitic, and abyssal peridotites. In: Carlson, R.W. (Ed.), The Mantle and Core. Elsevier, Amsterdam, pp. 103–170.

Bonatti, E., Hamlyn, P.R., Ottonello, G., 1986. Peridotites from the island of Zabargad (St. John), Red Sea; petrology and geochemistry. J. Geophys. Res. 21, 599–631.

Boyd, F.R., 1989. Compositional distinction between oceanic and cratonic lithosphere. Earth Planet. Sci. Lett. 96, 15–26.

Boyd, F.R., McCallister, R.H., 1976. Densities of fertile and sterile garnet peridotites. Geophys. Res. Lett. 3, 509–512.

Braun, J., Beaumont, C., 1989. A physical explanation of the relation between flank uplifts and the breakup unconformity at rifted continental margins. Geology 17, 760–764.

Brey, G.P., Doroshev, A.M., Girnis, A.V., Turkin, A.I., 1999. Garnet–spinel–olivine–orthopyroxene equilibria in the FeO–MgO–Al₂O₃–SiO₂–Cr₂O₃ system: I. Composition and molar volumes of minerals. Eur. J. Mineral. 11, 599–617.

Chazot, G., Charpentier, S., Kornprobst, J., Vannucci, R., Luais, B., 2005. Lithospheric mantle evolution during continental break-up: the West Iberia non-volcanic passive margin. J. Petrol. 46, 2527–2568.

Connolly, J.A.D., Petrini, K., 2002. An automated strategy for calculation of phase diagram sections and retrieval of rock properties as a function of physical conditions. J. Metamorph. Geol. 20, 697–708.

Dick, H.J.B., Bullen, T., 1984. Chromian spinel as petrogenetic indicator in abyssal and alpine-type peridotites and spatially associated lavas. Contrib. Mineral. Petrol. 86, 54–76.

Falvey, D.A., 1974. The development of continental margins in plate tectonic theory. APEA J. 14, 95–106.

Frey, F.A., John Suen, C., Stockman, H.W., 1985. The Ronda high temperature peridotite: geochemistry and petrogenesis. Geochim. Cosmochim. Acta 49, 2469–2491.

Girnis, A.V., Brey, G.P., Doroshev, A.M., Turkin, A.I., Simon, N., 2003. The system MgO–Al_2O_3–SiO_2–Cr_2O_3 revisited; reanalysis of Doroshev et al.'s (1997) experiments and new experiments. Eur. J. Mineral. 15, 953–964.

Green, D.H., Ringwood, A.E., 1967. The stability fields of aluminous pyroxene peridotite and garnet peridotite and their relevance in upper mantle structure. Earth Planet. Sci. Lett. 3, 151–160.

Green, D.H., Hibberson, W., 1970a. The instability of plagioclase in peridotite at high pressure. Lithos 3, 209–221.

Green, D.H., Ringwood, A.E., 1970b. Mineralogy of peridotitic compositions under upper mantle conditions. Phys. Earth Planet. Int. 3, 359–371.

Green, D.H., Liebermann, R.C., 1976. Phase equilibria and elastic properties of a pyrolite model for the oceanic upper mantle. Tectonophys 32, 61–92.

Hartz, E.H., Podladchikov, Y.Y., Medvedev, S., Faleide, J.I., Simon, N.S.C., 2007. Force, energy and mass balanced basin models: new concepts and Arctic examples. Geophys. Res. Abstr. 9, 10468.

Holland, T., Powell, R., 1998. An internally consistent thermodynamic data set for phases of petrological interest. J. Metamorph. Geol. 16, 309–343.

Huismans, R.S., Podladchikov, Y.Y., Cloetingh, S., 2001. Transition from passive to active rifting: Relative importance of asthenospheric doming and passive extension of the lithosphere. J. Geophys. Res. 106, 11271–11291.

Kaus, B.J.P., Connolly, J.A.D., Podladchikov, Y.Y., Schmalholz, S.M., 2005. Effect of mineral phase transitions on sedimentary basin subsidence and uplift. Earth Planet. Sci. Lett. 233, 213–228.

Klemme, S., 2004. The influence of Cr on the garnet–spinel transition in the Earth's mantle: experiments in the system MgO–Cr_2O_3–SiO_2 and thermodynamic modelling. Lithos 77, 639–646.

Klemme, S., O'Neill, H., 2000. The near-solidus transition from garnet lherzolite to spinel lherzolite. Contrib. Mineral Petrol 138, 237–248.

Kushiro, I., 1965. Clinopyroxene solid solutions at high pressure. Carnegie Inst. Washington Yearbook 64, 112–120.

Kushiro, I., Yoder Jr., H.S., 1966. Anorthite–forsterite and anorthite–enstatite reactions and their bearing on the basalt–eclogite transformation. J. Petrol. 7, 337–362.

MacGregor, I., 1974. The system MgO–Al_2O_3–SiO_2: solubility of Al_2O_3 in enstatite for spinel and garnet peridotite compositions. Am. Mineral. 59, 110–119.

McKenzie, D., 1978. Some remarks on the development of sedimentary basins. Earth Planet. Sci. Lett. 40, 25–32.

Müntener, O., Piccardo, G.B., 2003. Melt migration in ophiolitic peridotites: the message from Alpine–Apennine peridotites and implications for embryonic ocean basins. In: Dilek, Y., Robinson, P.T. (Eds.), Ophiolites in Earth History. The Geological Society of London, London, pp. 69–89.

O'Neill, H.S.C., 1981. The transition between spinel lherzolite and garnet lherzolite, and its use as a geobarometer. Contrib. Mineral. Petrol. 77, 185–194.

Pearson, D.G., Canil, D., Shirey, S.B., 2003. Mantle samples included in volcanic rocks: xenoliths and diamonds. In: Carlson, R.W. (Ed.), The Mantle and Core. Elsevier, Amsterdam, pp. 171–275.

Petrini, K.A.T.E., Connolly, J.A.D., Podladchikov, Y.Y., 2001. A coupled petrological–tectonic model for sedimentary basin evolution: the influence of metamorphic reactions on basin subsidence. Terra Nova 13, 354–359.

Podladchikov, Y.Y., Poliakov, A.N.B., Yuen, D.A., 1994. The effect of lithospheric phase transitions on subsidence of extending continental lithosphere. Earth Planet. Sci. Lett. 124, 95–103.

Podladchikov, Y.Y., Rüpke, L.H., Schmalholz, S.M., Simon, N.S.C., 2006. Late syn-rift (65–55 Ma) uplift in the Vøring Basin, Norwegian Sea — was it a 'hot' or a 'cold' event? EOS Trans. AGU 87 Abstract T52C-04.

Poudjom Djomani, Y.H., O'Reilly, S.Y., Griffin, W.L., Morgan, P., 2001. The density structure of subcontinental lithosphere through time. Earth Planet. Sci. Lett. 184, 605–621.

Presnall, D.C., Gudfinnsson, G.H., Walter, M.J., 2002. Generation of mid-ocean ridge basalts at pressures from 1 to 7 GPa. Geochim. Cosmochim. Acta 66, 2073–2090.

Ren, S., Faleide, J.I., Eldholm, O., Skogseid, J., Gradstein, F., 2003. Late Cretaceous–Paleocene tectonic development of the NW Vøring Basin. Mar. Petrol. Geol. 20, 177–206.

Ringwood, A., 1975. Composition and petrology of the earth's upper mantle. McGraw-Hill, London.

Ringwood, A.E., 1966. Chemical evolution of the terrestrial planets. Geochim. Cosmochim. Acta 30, 41–104.

Robertson, E., Birch, F., MacDonald, G.J.F., 1957. Experimental determination of jadeite stability relations to 25,000 bars. Am. J. Sci. 255, 115–137.

Robinson, J.A.C., Wood, B.J., 1998. The depth of the spinel to garnet transition at the peridotite solidus. Earth Planet. Sci. Lett. 164, 277–284.

Rüpke, L.H., Schmalholz, S.M., Schmid, D.W., Podladchikov, Y.Y., 2007. Automated thermotectono–stratigraphic basin reconstruction: Viking Graben case study. AAPG Bull. 92, 309–326.

Schutt, D.L., Lesher, C.E., 2006. Effects of melt depletion on the density and seismic velocity of garnet and spinel lherzolite. J. Geophys. Res. 111. doi:10.1029/2003JB002950.

Simon, N.S.C., Rüpke, L.H., Podladchikov, Y.Y., 2007. Quantifying the effect of mantle phase transitions and application to the Vøring basin, off-shore Norway, Abstr. AAPG Hedberg Conf. "Basin Modeling Perspectives: Innovative Developments and Novel Applications". The Hague, The Netherlands.

Walter, M., et al., 2002. Spinel–garnet lherzolite transition in the system CaO–MgO–Al_2O_3–SiO_2 revisited: an in situ X-ray study. Geochim. Cosmochim. Acta 66, 2109–2121.

Whitmarsh, R.B., Manatschal, G., Minshull, T.A., 2001. Evolution of magma-poor continental margins from rifting to seafloor spreading. Nature 413, 150–154.

Wood, B.J., Yuen, D.A., 1983. The role of lithospheric phase transitions on seafloor flattening at old ages. Earth Planet. Sci. Lett. 66, 303–314.

Yamasaki, T., Nakada, M., 1997. The effects of the spinel–garnet phase transition on the formation of rifted sedimentary basins. Geophys. J. Int. 130, 681–692.

Ziegler, P.A., Cloetingh, S., 2004. Dynamic processes controlling evolution of rifted basins. Earth Sci. Rev. 64, 1–50.